mathematics

MDPI

Article

Numerical Reconstruction of a Space-Dependent Reaction Coefficient and Initial Condition for a Multidimensional Wave Equation with Interior Degeneracy

Hamed Ould Sidi [1], Mahmoud A. Zaky [2,3], Rob H. De Staelen [4,5,*] and Ahmed S. Hendy [6,7]

1 Department of Mathematics, Faculty of Sciences, University of Nouakchott Al Aasriya, Nouakchott Bp 6093, Mauritania; hamedouldsidi@yahoo.fr
2 Department of Mathematics and Statistics, College of Science, Imam Mohammad Ibn Saud Islamic University (IMSIU), Riyadh 11432, Saudi Arabia; ma.zaky@yahoo.com
3 Department of Applied Mathematics, National Research Centre, Cairo 12622, Egypt
4 Beheer en Algemene Directie, Ghent University Hospital, Corneel Heymanslaan 10, B-9000 Ghent, Belgium
5 Research Department, Ghent University, Sint-Pietersnieuwstraat 25, B-9000 Ghent, Belgium
6 Department of Computational Mathematics and Computer Science, Institute of Natural Sciences and Mathematics, Ural Federal University, 19 Mira St., Yekaterinburg 620002, Russia; ahmed.hendy@fsc.bu.edu.eg
7 Department of Mathematics, Faculty of Science, Benha University, Benha 13511, Egypt
* Correspondence: rob.destaelen@ugent.be

Abstract: A simultaneous reconstruction of the initial condition and the space-dependent reaction coefficient in a multidimensional hyperbolic partial differential equation with interior degeneracy is of concern. A temporal integral observation is utilized to achieve that purpose. The well-posedness, existence, and uniqueness of the inverse problem under consideration are discussed. The inverse problem can be reformulated as a least squares minimization and the Fréchet gradients are determined, using the adjoint and sensitivity problems. Finally, an iterative construction procedure is developed by employing the conjugate gradient algorithm while invoking the discrepancy principle as a stopping criterion. Some numerical experiments are given to ensure the performance of the reconstruction scheme in one and two dimensions.

Keywords: wave problem; interior degeneracy; coefficient and initial function reconstruction; CGM

MSC: 93C20; 34K35; 93C95; 35L10

Citation: Sidi, H.O.; Zaky, M.A.; De Staelen, R.H.; Hendy, A.S. Numerical Reconstruction of a Space-Dependent Reaction Coefficient and Initial Condition for a Multidimensional Wave Equation with Interior Degeneracy. *Mathematics* **2023**, *11*, 3186. https://doi.org/10.3390/math11143186

Academic Editors: Yury Shestopalov and Victor Orlov

Received: 22 April 2023
Revised: 8 July 2023
Accepted: 10 July 2023
Published: 20 July 2023

1. Introduction

Numerous significant applications in cosmology [1], data science [2], remote sensing [3], medicine [4], and geophysics [5] are modeled in inverse problems involving the determination of unknown coefficients of partial differential equations based on limited information about the system over a finite period. Degenerate wave models are gaining more focus these days in many physical applications [6–8]. A survey of the numerical techniques that have been applied to direct and inverse problems with integer or fractional order derivatives indicates a lot of focus in recent days [9–11]. A reconstruction of missing sole terms in different styles of time-dependent fractional diffusion problems has been seen in [12,13].

The problem under consideration invokes the one proposed in [14] in which the reconstruction is only targeted to the potential term. We address here the reconstruction

of two factors (initial condition and potential) in a multidimensional wave problem with interior degeneracy.

$$\begin{cases} \partial_{tt}\varphi - \nabla\cdot(a\,\nabla\varphi) + b\,\varphi &= Q & \text{in} & I, \\ \varphi &= 0 & \text{in} & (\mathbb{R}^d\backslash\chi)\times(0,S], \\ \varphi(\cdot,0) &= u_0(x) & \text{in} & \chi, \\ \varphi_t(\cdot,0) &= v_0(x) & \text{in} & \chi, \end{cases} \tag{1}$$

where $I := \chi \times (0,S]$. Endowed with the final observation data $\varphi(\cdot,S)$ in the domain χ, where $S > 0$ and $\chi \subset \mathbb{R}^d (d \geq 1)$, $Q \in \mathcal{L}^2(\chi\times(0,S))$, $b \in \mathcal{L}^2(\chi)$ $isa \in C^1(\chi)$ a function that degenerates into a point x_0 inside the spatial domain χ with $\{1 \geqslant a(x) \geqslant 0, \quad \forall x \in \chi\}$. The Hilbert space is defined as

$$\mathcal{H}_a^1(\chi) := \left\{\varphi \in W_0^{1,1}(\chi) \,:\, \sqrt{a}\nabla\varphi \in \mathcal{L}^2(\chi)\right\},$$

with the inner product

$$\langle\varphi, v\rangle_{\mathcal{H}_a^1} := \int_\chi a\nabla\varphi\cdot\nabla v\,dx + \int_\chi \varphi v\,dx.$$

An important application of the inverse problem (1) is to distinguish between various types of seismic events, such as implosion, explosion, or earthquake, which generate waves that propagate through the Earth and can be recorded using seismometers. In [15], a seismic source modeled as a point moment tensor forcing in the elastic wave equation for the displacement was estimated by minimizing the gap between the time-dependent measured/recorded and computed waveforms (see [16]). The weak formulation of (1) is:

$$\int_\chi \partial_{tt}\varphi v\,dx + \int_\chi a(x)\nabla\varphi\cdot\nabla v\,dx + \int_\chi b\,\varphi v\,dx = \int_\chi Qv\,dx, \;\; \forall v \in \mathcal{H}_0^1(\chi). \tag{2}$$

In the literature, the inverse problem of determining the coefficient $b(x)$ over a large scale from time $t = S$ and its time-integratation for temperature, among other data, has been studied and used to prove its existence and uniqueness when the source term Q, the Dirichlet boundary conditions, and the initial condition u_0 are known [17–20].

In addition, several numerical methods have been proposed. Examples include the standard regularization method of the Tikhonov type [21], the method of Armijo combined with the finite element method [22], the (NAG E04FCF) combined with the method of finite differences (FDM) [23], and the conjugate gradient method (CGM) [24] to reconstruct the coefficient $b(x)$ numerically from the additional measurements.

Extensive research has been conducted on the inverse problem of determining the initial condition from time-integral temperature measurements and a final instant when the reaction potential and the source term are known (see, for example, [25,26]).

In this paper, we study the generalization of the conditions used in [27], which amounts to knowing the direct solution at certain instants of the time domain and at its end. This is difficult in practice to implement with precision at recordings with an average time, which reduces the possibility of significant measurement errors in the direct solution φ. More specifically, using the average weighted integral observations given in (3) and (4), we study the inverse problem to determine the pair $(b(x)$ and $u_0(x))$ in (1). Let $\rho_1(t), \rho_2(t)$ be two approximations to the delta function at $t = S$, such that $\rho_1(t), \rho_2(t) \in C^1(0,T)$, which are given, and $\psi_1(x)$ and $\psi_2(x)$ are the average weighted integral observations that are also given. Let

$$\int_0^S \rho_1(t)\varphi(x,t)\,dt = \psi_1(x), \;\; x \in \chi \tag{3}$$

$$\int_0^S \rho_2(t)\varphi(x,t)\,dt = \psi_2(x), \;\; x \in \chi. \tag{4}$$

Taking into account the generalizations of the final observations $\varphi(t = S)$, the integral observations (3) and (4) can be thought of in this way. However, note that the selection of the weighted functions (3) and (4) has a crucial role in obtaining the relevant data to recover the two unknown values $(b(x), u_0)$; for more information, refer to [28]. On the other hand, in the literature, the determination of the reaction potential and the source term have been studied from the final observation of time in [27] and the measurement of the integral observation in time in [29] for non-degenerate parabolic problems. In the inverse problems (1), (3), and (4), these approaches can also be used to simultaneously calculate the response coefficient $b(x)$ and the initial condition $u_0(x)$.

The manuscript is arranged to have the uniqueness of the inverse problem in Section 2. The stability and the regularity results, the proof of the Fréchet differentiability of the objective functional, and the conjugate gradient and sensitivity problems are presented in Section 3. Using the conjugate gradient method (CGM) regularized by the discordance principle [30], the inverse problem is solved numerically in a stable way. Section 4 is devoted to the numerical simulations and their good agreement with the theoretical analysis. The well-posedness of the direct problem of (1) is discussed in the following theorem.

Theorem 1. *Assume that* $v_0 \in \mathcal{L}^2(\chi)$, $0 \leq b \in C^1$ *and* $u_0 \in \mathcal{H}_a^1(\chi)$, $Q \in \mathcal{L}^2(0, S, \chi)$. *The problem (1) has the following unique weak solution*

$$\varphi \in \mathcal{X}_0 = \mathcal{L}^2\Big(0, S; \mathcal{H}_a^1(\chi)\Big) \cap \mathcal{L}^\infty\Big(0, S; \mathcal{L}^2(\chi)\Big)\ ,\ \partial_t \varphi \in \mathcal{L}^2(0, S; \mathcal{L}^2(\chi)), \tag{5}$$

with

$$\begin{aligned} &\sup_{t\in[0,S]} \| \varphi(t) \|^2_{\mathcal{L}^2(\chi)} + \| \partial_t \varphi \|^2_{\mathcal{L}^2(0,S;\mathcal{L}^2(\chi))} + \| \sqrt{a(x)}\nabla \varphi \|^2_{\mathcal{L}^2(0,S;\mathcal{L}^2(\chi))} \\ &\leqslant C\Big(\| u_0 \|^2_{\mathcal{H}_a^1(\chi)} + \| v_0 \|^2_{\mathcal{L}^2(\chi)} + \| Q \|^2_{\mathcal{L}^2(0,S;\mathcal{L}^2(\chi))} \Big). \end{aligned} \tag{6}$$

The constant C depends on χ *and* S.

Proof. The proof of the following theorem relies on the outlines used to prove the existence and uniqueness theorem for the degenerate linear viscose-elastic problem presented in [31]. □

2. Well-Posedness of the Inverse Problem

Firstly, we introduce the following admissible set:

$$\mathcal{E} = \{b \in \mathcal{L}^\infty(\chi) : 0 \leq b_1 \leq b(x) \leq b_2,\ \ a.e.\ \ x \in \chi\}$$

A reformulation of the inverse problems (1), (3), and (4) as a nonlinear non-classical parabolic problem is targeted to simplify the proof of existence and uniqueness. By multiplying the first equation in (1) by $\rho_1(t)$ and $\rho_2(t)$, respectively, integrating the resulting relations with respect to t from 0 to S, and using (3) and (4), we have

$$-\rho_i'\varphi(x,T) + \rho_i' u_0(x) + \int_0^T \rho_i''\varphi(x,t)\,dt = \nabla.\Big(a.\nabla\psi_i\Big) - b(x)\varphi(x,t) + \int_0^T \rho_i\, Q(x,t)\,dt \tag{7}$$

Using (7), we have

$$q(x) = A_2(x)(a_1(x) + \bar{\varphi}_1(x)) - A_1(x)(a_2(x) + \bar{\varphi}_2(x)) \tag{8}$$

$$u_0(x) = B_2(x)(a_1(x) + \bar{\varphi}_1(x)) - B_1(x)(a_2(x) + \bar{\varphi}_2(x)) \tag{9}$$

where

$$\begin{cases} a_i(x) &= \nabla.\Big(a(x)\nabla\psi_i\Big) + \int_0^S Q(x,t)\rho_i(t)\,dt \\ A_i(x) &= \dfrac{\rho_i'(0)}{\psi_2\rho_1(t) - \psi_1\rho_2(t)} \\ B_i(x) &= \dfrac{\psi_i(x)}{\psi_2\rho_1(t) - \psi_1\rho_2(t)} \\ \bar{\varphi}_i &= \rho_i'\varphi(x,T) - \int_0^T \rho_i''\varphi(x,t)\,dt \end{cases}$$

We introduce the following assumptions:

(a) $\psi_1, \psi_2 \in H^2(\chi) \cap L^\infty(\chi)$ and $\rho_1, \rho_2 \in C^2[0,T]$;
(b) $\psi_2\rho_1(t) - \psi_1\rho_2(t) \neq 0$;
(c) $A_1a_1 - A_1a_2 \geq K_1$ and $B_2a_1 - B_1a_2 \leq K_2$ a.e. in $\bar{\chi}$, for some positive constants K_1 and K_1.

Inserting (8) and (9) into (1), we obtain

$$\begin{cases} \partial_{tt}\varphi - \nabla\cdot(a\,\nabla\varphi) + A_2(x)(a_1(x) + \bar{\varphi}_1(x)) - A_1(x)(a_2(x) + \bar{\varphi}_2(x))\,\varphi = 0 \ \text{ in } \ I, \\ \varphi = 0 \ \text{ in } \ (\mathbb{R}^d\backslash\chi)\times(0,S], \\ \varphi_t(\cdot,0) = 0 \ \text{ in } \ \chi, \\ \varphi(\cdot,0) = B_2(x)(a_1(x) + \bar{\varphi}_1(x)) - B_1(x)(a_2(x) + \bar{\varphi}_2(x)) \ \text{ in } \ \chi, \end{cases} \tag{10}$$

Thus, the solution to inverse problems (1), (3), and (4) is equivalent to obtaining the solution $\varphi(x,t)$ to the nonlinear parabolic problem (10). Utilize the technique in [19], and consider the following two auxiliary hyperbolic problems:

$$\begin{cases} \partial_{tt}\Phi - \nabla\cdot(a\,\nabla\Phi) + \Big(A_2(x)a_1(x) - A_1(x)a_2(x)\,\Phi = Q \ \text{ in } \ I, \\ \Phi = 0 \ \text{ in } \ (\mathbb{R}^d\backslash\chi)\times(0,S], \\ \Phi_t(\cdot,0) = 0 \ \text{ in } \ \chi, \\ \Phi(\cdot,0) = 0 \ \text{ in } \ \chi, \end{cases} \tag{11}$$

and

$$\begin{cases} \partial_{tt}\Psi - \nabla\cdot(a\,\nabla\Psi) + A_2a_1 - A_1a_2 + c\Big(A_2(\bar{\Psi}_1 + \bar{\Phi}_1) - A_1(\bar{\Psi}_2 + \\ \bar{\Phi}_2)\Big)\Psi - c\Big(A_2(\bar{\Psi}_1 + \bar{\Phi}_1) - A_1(\bar{\Psi}_2 + \bar{\Phi}_2)\Big)\Phi\,\Phi = 0 \ \text{ in } \ I, \\ \Psi = 0 \ \text{ in } \ (\mathbb{R}^d\backslash\chi)\times(0,S], \\ \Psi_t(\cdot,0) = 0 \ \text{ in } \ \chi, \\ \Psi(\cdot,0) = B_2a_1 - B_1a_2 + c\Big(B_2(\bar{\Psi}_1 + \bar{\Phi}_1) - B_1(\bar{\Psi}_2 + \\ \bar{\Phi}_2)\Big)\Psi - c\Big(B_2(\bar{\Psi}_1 + \bar{\Phi}_1) - B_1(\bar{\Psi}_2 + \bar{\Phi}_2)\Big)\Phi \ \text{ in } \ \chi, \end{cases} \tag{12}$$

where c is a Lipschitz continuous function on $\mathbb{R}$ defined by

$$c(x) = \begin{cases} x & if \quad |x| \leq K_0 \\ K_0 & if \quad x > K_0 \\ -K_0 & if \quad x < -K_0 \end{cases}$$

and

$$\bar{\Phi}_i = \rho_i'(t)\Phi(x,T) - \int_0^T \rho_i''\Phi(x,t)\,dt, \ \ \bar{\Psi}_i = \rho_i'(t)\Psi(x,T) - \int_0^T \rho_i''\Psi(x,t)\,dt \tag{13}$$

Therefore Φ, and Ψ, satisfy

$$|\Phi(x,t)| \leq L_2 \ \ a.e. \ \ (x,t) \in I, \ \ |\Psi(x,t)| \leq L_3 \ \ a.e. \ \ (x,t) \in I, \tag{14}$$

with $L_1 > 0$.

To prove the existence and uniqueness of the solution to the inverse problems (1), (3), and (4). We set

$$K_3 := |\rho_1'(t)| + |\rho_2'(t)| + \int_0^S \rho_1'\,dt + \int_0^S \rho_2'\,dt$$

$$K_4 = \max_{x\in\bar{\chi}}\{|A_1|, |A_2|, |B_1|, |B_2|\} \tag{15}$$

$$L_3 := \frac{2K_3K_4(L_1+L_2)}{K_1 - 2K_3K_4(L_1+L_2)} \tag{16}$$

Theorem 2. *Let $a, v_0, \psi_1, \psi_2 \in L^\infty(\chi)$, and $\rho_1, \rho_2 \in L^\infty(0,S), Q \in L^\infty(I)$, and, for the functional spaces inverse problem solution, we put $\mathcal{Y}_0 = \mathcal{L}^2\big(0,S;\mathcal{H}_a^1(\chi)\big) \cap \mathcal{L}^\infty\big(0,S;\mathcal{L}^2(\chi)\big) \cap H^{2,1}(I)$.*

Suppose that assumptions (a)–(c) are satisfied. Assume that there exists a number $K_0 \in (0, K_1)$ satisfying

$$2K_3K_4(L_1+L_2) \le K_0, \;\; L_3 < 1. \tag{17}$$

Then, there exists at most one solution $(\varphi(x,t), b(x), u_0(x)) \in \mathbb{X}_0 \times L^\infty(\chi) \times L^\infty(\chi)$ and $b(x) > 0$ a.e. $x \in \bar{\chi}$ to the inverse problems (1), (3), and (4).

Proof. Using (13), we have

$$|\bar{\Phi}_1| \le \Big(|\rho_1'(t)| + \int_0^T |\rho_1''|\,dt\Big)\|\Phi\|_{L^\infty(\chi)} \le K_3L_2 \tag{18}$$

Likewise, we have $|\bar{\Psi}_2| \le K_3L_2$, $|\bar{\Psi}_2| \le K_3L_1$, which imply that

$$|\bar{\Phi}_i + \bar{\Psi}_i +| \le K_3(L_1+L_2), \;\; for \;\; i = 1,2.$$

$$|A_2(\bar{\Psi}_1+\bar{\Phi}_1) - A_1(\bar{\Psi}_2+\bar{\Phi}_2)| \le K_3(L_1+L_2)(|A_1|+|A_2|) \le 2K_3K_4(N_1+N_2),$$
$$|B_2(\bar{\Psi}_1+\bar{\Phi}_1) - B_1(\bar{\Psi}_2+\bar{\Phi}_2)| \le K_3(L_1+L_2)(|B_1|+|B_2|) \le 2K_3K_4(N_1+N_2),$$

Using inequality (17) and the definition of function $c(.)$, we obtain

$$c\Big(A_2(\bar{\Psi}_1+\bar{\Phi}_1) - A_1(\bar{\Psi}_2+\bar{\Phi}_2)\Big) = A_2(\bar{\Psi}_1+\bar{\Phi}_1) - A_1(\bar{\Psi}_2+\bar{\Phi}_2),$$

$$c\Big(B_2(\bar{\Psi}_1+\bar{\Phi}_1) - B_1(\bar{\Psi}_2+\bar{\Phi}_2)\Big) = B_2(\bar{\Psi}_1+\bar{\Phi}_1) - B_1(\bar{\Psi}_2+\bar{\Phi}_2).$$

Hence, problem (12) becomes

$$\begin{cases} \partial_{tt}\Psi - \nabla\cdot(a\,\nabla\Psi) + A_2a_1 - A_1a_2 + \Big(A_2(\bar{\Psi}_1+\bar{\Phi}_1) - A_1(\bar{\Psi}_2+\bar{\Phi}_2)\Big)\Psi \\ \qquad - \Big(A_2(\bar{\Psi}_1+\bar{\Phi}_1) - A_1(\bar{\Psi}_2+\bar{\Phi}_2)\Big)\Phi = 0 \;\text{ in }\; I, \\ \Psi = 0 \;\text{ in }\; (\mathbb{R}^d\backslash\chi)\times(0,S], \\ \Psi_t(\cdot,0) = 0 \;\text{ in }\; \chi, \\ \Psi(\cdot,0) = B_2a_1 - B_1a_2 + \Big(B_2(\bar{\Psi}_1+\bar{\Phi}_1) - B_1(\bar{\Psi}_2+ \\ \bar{\Phi}_2)\Big)\Psi - \Big(B_2(\bar{\Psi}_1+\bar{\Phi}_1) - B_1(\bar{\Psi}_2+\bar{\Phi}_2)\Big)\Phi \;\text{ in }\; \chi, \end{cases} \tag{19}$$

By taking $\varphi(x,t) = \Psi(x,t) + \Phi(x,t)$, it is easy to obtain that φ satisfies the estimate

$$|\varphi(x,t)| \le L_1 + L_2 \;\; a.e. \;\; (x,t) \in \bar{I} \tag{20}$$

Let $w(x,t)$ and $v(x,t)$ be two solutions to problem (10), and let $w(x,t) = w(x,t) - v(x,t)$. Then, $\varphi_3(x,t)$, satisfies the following problem:

$$\begin{cases} \partial_{tt} z - \nabla \cdot (a \nabla z) + \Big(A_2 a_1 - A_1 a_2 + A_2(\bar{w}_1 - A_1(\bar{w}_2\Big) z \\ \qquad - \Big(A_2(\bar{z}_1 - A_2(\bar{z}_2) v = 0 \text{ in } I, \\ \qquad z = 0 \text{ in } (\mathbb{R}^d \backslash \chi) \times (0, S], \\ \qquad z_t(\cdot, 0) = 0 \text{ in } \chi, \\ \qquad z(\cdot, 0) = \Big(B_2(\bar{z}_1 - B_1(\bar{z}_2\Big) \text{ in } \chi, \end{cases} \tag{21}$$

with

$$\bar{w}_i = \rho_i'(t) w(x,T) - \int_0^T \rho_i'' w(x,t), \;\; \bar{v}_i = \rho_i'(t) v(x,T) - \int_0^T \rho_i'' v(x,t).$$

Using (17) and (18), we obtain

$$\begin{aligned} |A_2 a_1 - A_1 a_2 + A_2 \bar{w}_1 - A_1 \bar{w}_2| &\geq K_1 - \max_{x \in \bar{\chi}} |A_2 \bar{w}_1 - A_1 \bar{w}_2| \\ &\geq K_1 - 2K_3 K_4 (L_1 + L_2) > K_0 - 2K_3 K_4 (L_1 + L_2) \geq 0, \end{aligned}$$

and, as $|\bar{z}_i| \leq K_3 \|\bar{z}_i\|_{L^2(I)}$ for $i = 1, 2$, then

$$\max |A_2 \bar{z}_1 - A_1 \bar{z}_2|, |B_2 \bar{z}_1 - B_1 \bar{z}_2| \leq 2K_3 K_4 \|z\|_{L^\infty(I)}$$

$$\|z\|_{L^\infty(I)} \leq \frac{2K_3 K_4 \|z\|_{L^\infty(I)} \|v\|_{L^\infty(I)}}{K_1 - 2K_3 K_4 (L_1 + L_2)} \leq L_3 \|z\|_{L^\infty(I)}.$$

Using the fact that $L_3 < 1$, we obtain that $\|z\|_{L^\infty(I)} = 0$. This implies the uniqueness of the solution to problem (10). This means that the potential $b(x)$ given by (8) and the initial condition $u_0(x)$ given by (9) only satisfy the inverse problems (1), (3), and (4). The proof is completed. □

In this paper, we generalize the constant-time observations to mean-time records, which can be difficult to achieve in practice, and these records smooth out potentially large measurement errors in the direct solution φ. More precisely, we are looking for the triple $(\varphi(x,t), b(x), u_0(x))$ of problem (1) with average weighted integral observations. Let $\varphi(x,t;b,u_0)$ be the solution to the direct problem (1). Now, let us reformulate our inverse problem as an optimization problem. In reality, the average weighted integral observations $\psi_1, \psi_2 \in \mathcal{L}^\infty(\chi)$, given in (3) and (4), respectively, may contain noise. Due to the poor posing of the inverse problem, which causes tiny inaccuracies in the input data (3) and (4) to lead to substantial errors in the output coefficients $b(x)$ and $u_0(x)$. This creates the main challenge numerically in the reconstruction of the solution. Numerically, we are looking for an approximation of the answer using measurements with noise. Let us consider $\psi_1^\delta, \psi_2^\delta \in \mathcal{L}^\infty(\chi)$, satisfying

$$\left\| \psi_i^\delta - \psi \right\|^2_{\mathcal{L}^2(\chi)} \leq \delta, \;\; \textit{for} \;\; i = 1, 2. \tag{22}$$

Hence, we will simultaneously reconstruct the coefficient $b(x)$ and the condition $u_0(x)$ under the following noisy data: $(\psi_1^\delta(x), (\psi_2^\delta(x))$

$$\int_0^S \rho_1(t) \varphi(x,t)\, dt = \psi_1^\delta(x), \;\; x \in \chi, \tag{23}$$

$$\int_0^S \rho_2(t) \varphi(x,t)\, dt = \psi_2^\delta(x), \;\; x \in \chi. \tag{24}$$

We minimize the objective functional $\mathcal{M}[b,u_0]:\mathcal{E}\times\mathcal{L}^2(\chi)\to\mathbb{R}$ defined in (25) to obtain the solution to the inverse problem

$$\mathcal{M}[b,u_0]=\frac{1}{2}\Big\|\int_0^S\rho_1(t)\varphi(\cdot,b,u_0)\,dt-\psi_1^\delta\Big\|^2_{\mathcal{L}^2(\chi)}+\frac{1}{2}\Big\|\int_0^S\rho_2(t)\varphi(\cdot,b,u_0)\,dt-\psi_2^\delta\Big\|^2_{\mathcal{L}^2(\chi)}. \tag{25}$$

In this paper, our technique does not depend on the "regularize then discretize approach"; more precisely, we adopt the approach used in [32].

Theorem 3. *The optimization problem in (25) admits at least one solution.*

Proof. We know that $\inf_{\mathcal{E}\times\mathcal{L}^2(\chi)}\mathcal{M}[b,u_0]=:\mathcal{M}_0\geq 0$. This gives the existence of a minimizing sequence $\{(b^n,u_0^n):n\in\mathbb{N}\}\subset\mathcal{E}\times\mathcal{L}^2$ such that

$$\lim_{n\to\infty}\mathcal{M}[b^n,u_0^n]=\mathcal{M}_0.$$

Hence, the subsequence $\{(b^n,u_0^n):n\in\mathbb{N}\}$ is uniformly bounded in $\mathcal{L}^\infty(\chi)\times\mathcal{L}^2(\chi)$, which proves the existence of the subsequence (b^n,u_0^n) which converges weakly to (b^*,u_0^*) in $\mathcal{L}^\infty(\chi)\times\mathcal{L}^2(\chi)$. Using estimate (5), we find that the sequence $\{\varphi^n=\varphi(b^n,u_0^n):n\in\mathbb{N}\}$ is uniformly bounded in $H_0^1(I)$, So we can extract a subsequence $\{\varphi^n:n\in\mathbb{N}\}$, which converges weakly to $\varphi^*\in H_0^1(I)$ in $H_0^1(I)$.

Let $\theta\in H_0^1(I)$ such that $\theta(.,T)=0$. The variational formulation of problem (1) for (φ^n,b^n,u_0^n) gives

$$\int_I\varphi^n\partial_{tt}\theta+\int_I a\nabla\varphi^n\cdot\nabla\theta+\int_I b^n\varphi^n\theta=\int_I Q\theta+\int_I u_0^n\partial_t\theta(x,0). \tag{26}$$

We can write $\int_I b^n\varphi^n\theta=\int_I b^*\varphi^n\theta+\int_I(b^n-b^*)\varphi^n\theta$. Using estimate (5) and the fact that b^n converges weakly to b^* in $\mathcal{L}^\infty(\chi)$, we find that $\int_I(b^n-b^*)\varphi^n\theta\to 0$. Consequently, by letting n tend to infinity in (26), we obtain

$$\int_I\varphi^*\partial_{tt}\theta+\int_I a\nabla\varphi^*\cdot\nabla\theta+\int_I b^*\varphi^*\theta=\int_I Q\theta+\int_I\varphi_0^*\partial_t\theta(x,0),$$

and, since H_0^1 injects into $\mathcal{L}^2(I)$, and the solution to the direct problem is unique, we deduce that $\varphi^*=\varphi(b^*,u_0^*)$. Now, by the weak lower semi-continuity of the norm, we have

$$\begin{aligned}\mathcal{M}[b^*,u_0^*]&=\frac{1}{2}\Big\|\int_0^S\rho_1(t)\varphi(\cdot,t)\,dt-\psi_1^\delta\Big\|^2_{\mathcal{L}^2(\chi)}+\frac{1}{2}\Big\|\int_0^S\rho_2(t)\varphi(\cdot,t)\,dt-\psi_2^\delta\Big\|^2_{\mathcal{L}^2(\chi)}\\&\leq\frac{1}{2}\lim_{n\to\infty}\Big\|\int_0^S\rho_1(t)\varphi^n(\cdot,t)\,dt-\psi_1^\delta\Big\|^2_{\mathcal{L}^2(\chi)}+\frac{1}{2}\lim_{n\to\infty}\Big\|\int_0^S\rho_2(t)\varphi^n(\cdot,t)\,dt-\psi_2^\delta\Big\|^2_{\mathcal{L}\mathcal{L}^2(\chi)}\\&\leq\liminf_{n\to\infty}\mathcal{M}[b^n,u_0^n]=\inf_{\mathcal{E}\times\mathcal{L}^2(\chi)}\mathcal{M}[b,u_0].\end{aligned}$$

This shows that (b^*,u_0^*) is a minimizer of (25) on the set $\mathcal{E}\times\mathcal{L}^2(\chi)$. □

To calculate the gradient of the functional $\mathcal{M}$, we use the conjugate gradient method introduced in Section 3. First, we show that this functional $\mathcal{M}$ is differentiable as stated in the following lemma:

Lemma 1. *Let the coefficient b and the initial condition be perturbed by a small δb and δu_0, with $(b+\delta b,u_0+\delta u_0\in\mathcal{E}\times\mathcal{L}^2(\chi)$, and let φ be the weak solution to (1) corresponding to (b,u_0). The function $\mathcal{E}\times\mathcal{L}^2(\chi)\to H_0^1(I)\times H_0^1(I)$ continues, i.e.,*

$$\Big\|\varphi(b+\delta b,u_0)-\varphi(b,u_0)\Big\|_{\mathcal{L}^2(0,T,H_0^1(\chi))}\leq c\Big\|\delta b\Big\|_{\mathcal{L}^\infty(\chi)}, \tag{27}$$

$$\left\|\varphi(b,u_0+\delta u_0)-\varphi(b,u_0)\right\|_{\mathcal{L}^2(0,T,H_0^1(\chi))}\leq c\left\|\delta u_0\right\|_{\mathcal{L}^2(\chi)}. \tag{28}$$

Proof. The proof is very simple. Just use estimate (5) and replace φ with $\varphi(b+\delta b,u_0)$ and $\varphi(b,u_0+\delta u_0)$ in (1). □

We rely on the following lemma to show the differentiability of the map $u\to\varphi(b,u_0)$.

Lemma 2. *Assume that $(b,u_0)\in\mathcal{E}\times\mathcal{L}^2(\chi)$. The map $(b,u_0)\to u(b,u_0)$ is Fréchet differentiable; more precisely, there are two operators $\mathcal{O}_b,\mathcal{O}_{u_0}:\mathcal{E}\times\mathcal{L}^2\to H_0^1(I)\times H_0^1(I)$, such that*

$$\lim_{\left\|\delta b\right\|_{\mathcal{L}^\infty(\chi)}\to 0}\frac{\left\|\varphi(b+\delta b,u_0)-\varphi(b,u_0)-\mathcal{O}_b\delta b\right\|_{\mathcal{L}^2(0,T,H_0^1(\chi))}}{\left\|\delta b\right\|_{\mathcal{L}^\infty(\chi)}}=0, \tag{29}$$

$$\lim_{\left\|\delta u_0\right\|_{\mathcal{L}^2(\chi)}\to 0}\frac{\left\|\varphi(b,u_0+\delta u_0)-\varphi(b,u_0)-\mathcal{O}_{u_0}\delta u_0\right\|_{\mathcal{L}^2(0,T,H_0^1(\chi))}}{\left\|\delta b\right\|_{\mathcal{L}^2(\chi)}}=0. \tag{30}$$

Proof. Let $b,\delta b\in\mathcal{E}$, and $\varphi(b,u_0)$ be the solution to problem (1). We can verify that φ satisfies the following problem:

$$\begin{cases}\partial_{tt}\varphi_b-\nabla\cdot(a\,\nabla\varphi_b)+b\,\varphi_b+\delta b\,\varphi(b,u_0) &= 0 \text{ in } I,\\ \varphi_b &= 0 \text{ in } (\mathbb{R}^d\backslash\chi)\times(0,S],\\ \varphi_b(\cdot,0) &= 0 \text{ in } \chi,\\ \varphi_t(\cdot,0) &= 0 \text{ in } \chi,\end{cases} \tag{31}$$

Then, problem (31) has a unique solution φ_b which depends linearly on δb. Let $z_b:=\varphi(b+\delta b,u_0)-\varphi(b,u_0)-\mathcal{O}_b\delta b=\delta\varphi_b-\varphi_b$. So, $\delta\varphi_b$ satisfies the following problem

$$\begin{cases}\partial_{tt}\delta\varphi_b-\nabla\cdot(a\,\nabla\delta\varphi_b)+b\,\delta\varphi_b+\delta b(\delta\varphi_b+\varphi(b,u_0)) &= 0 \text{ in } I,\\ \delta\varphi_b &= 0 \text{ in } (\mathbb{R}^d\backslash\chi)\times(0,S],\\ \delta\varphi_b(\cdot,0) &= 0 \text{ in } \chi,\\ \delta(\varphi_b)_t(\cdot,0) &= 0 \text{ in } \chi.\end{cases} \tag{32}$$

Using (31) directly shows that z verifies □

$$\begin{cases}\partial_{tt}z_b-\nabla\cdot(a\,\nabla z_b)+b\,z_b+\delta b\delta\varphi_b &= 0 \text{ in } I,\\ z_b &= 0 \text{ in } (\mathbb{R}^d\backslash\chi)\times(0,S],\\ z_b(\cdot,0) &= 0 \text{ in } \chi,\\ (z_b)_t(\cdot,0) &= 0 \text{ in } \chi.\end{cases} \tag{33}$$

Now, the application of estimate (5) to (33) gives

$$\left\|z_b\right\|_{\mathcal{L}^2(0,S,H_a^1(\chi))}\leq c_{b,u_0}\left\|\delta b\,\delta\varphi_b\right\|_{\mathcal{L}^2(I)}\leq c_{b,u_0}\left\|\delta b\right\|_{\mathcal{L}^\infty(I)}\left\|\delta\varphi_b\right\|_{\mathcal{L}^2(I)}\leq c_{b,u_0}\left\|\delta b\right\|_{\mathcal{L}^\infty(I)}\left\|\delta\varphi_b\right\|_{\mathcal{L}^2(0,S,H_a^1(\chi))}.$$

From (27), we conclude that

$$\left\|\varphi(b+\delta b,u_0)-\varphi(b,u_0)-\mathcal{O}_b\delta b\right\|_{\mathcal{L}^2(0,S,H_a^1(\chi))}\leq c_{b,u_0}\left\|\delta b\right\|^2_{\mathcal{L}^\infty(\chi)}.$$

Hence, the map $(b, u_0) \to \varphi(b, u_0)$ is Fréchet differentiable. This shows relation (29). Now, let $\delta\varphi_{u_0} = \varphi(b, u_0 + \delta u_0) - \varphi(b, u_0)$ be the solution to the problem

$$\begin{cases} \partial_{tt}\varphi_{u_0} - \nabla \cdot (a\,\nabla\varphi_{u_0}) + b\,\varphi_{u_0} + b\,\delta\varphi_b &= 0 \quad \text{in} \quad I, \\ \varphi_{u_0} &= 0 \quad \text{in} \quad (\mathbb{R}^d \backslash \chi) \times (0, S], \\ \delta\varphi_{u_0}(\cdot, 0) &= 0 \quad \text{in} \quad \chi, \\ \delta\partial_t\varphi_{u_0}(\cdot, 0) &= 0 \quad \text{in} \quad \chi. \end{cases} \tag{34}$$

In the same way, we can directly prove (30) for the coefficient b.

To calculate the gradient of $\nabla\mathcal{M}[b, u_0$, we need the following lemma, which gives the existence and uniqueness of the following adjoint problem of (1)

$$\begin{cases} -\partial_{tt}p - \nabla \cdot (a\,\nabla p) + b\,p &= \displaystyle\sum_{k=1}^{2} \rho_k(t)\Big(\int_0^S \rho_k\varphi(x,\tau)\,d\tau - \psi_k^\delta\Big) \quad \text{in} \quad I, \\ p &= 0 \quad \text{in} \quad (\mathbb{R}^d \backslash \chi) \times (0, S], \\ p(\cdot, 0) &= 0 \quad \text{in} \quad \chi, \\ \partial_t p(\cdot, 0) &= 0 \quad \text{in} \quad \chi. \end{cases} \tag{35}$$

Lemma 3. *Assume that $\rho_1, \rho_2 \in \mathcal{L}^\infty(\chi)$ and $b \in \mathcal{L}^\infty(\chi), \psi_1, \psi_2 \in \mathcal{L}^\infty(0, S)$. Based on these assumptions, problem (35) admits a unique solution. Moreover, there is $c' > 0$ such that*

$$\Big\|p\Big\|_{\mathcal{L}^2(I)} \le c' \sum_{k=1}^{2} \Big\|\rho_k\Big\|_{\mathcal{L}^\infty(0,S)} \Big(\Big\|\psi_k^\delta\Big\|_{\mathcal{L}^\infty(\chi)} + \Big\|\rho_k\Big\|_{\mathcal{L}^\infty(0,S)} \Big\|\varphi\Big\|_{\mathcal{L}^\infty(\mathbf{I})}\Big). \tag{36}$$

Proof. To show the existence and uniqueness of p, we use the same approach for problem (1). Multiplying both sides of the first equation of (35) by p_t and integrating it over χ, we obtain

$$\int_\chi \partial_{tt}p\,\partial_t p - \int_\chi \nabla \cdot (a(\nabla\, p)\partial_t p + \int_\chi b\,p = \int_\chi \sum_{k=1}^{2} \rho_k(t)\Big(\int_0^S \rho_k\varphi(x,\tau)\,d\tau - \psi_k^\delta\Big)\partial_t p.$$

Now, we integrate for $t \in [0, S]$, and we use the fact that $p(x,t) = \displaystyle\int_0^t \partial_t p(x,\tau)\,d\tau + p(x,0)$ to obtain

$$\Big\|p\Big\|^2_{\mathcal{L}^2(I)} + \int_I a(\nabla\,\varphi)^2 + \int_I b\,p^2 \le c' \sum_{k=1}^{2} \int_I p\rho_k(t)\Big(\int_0^S \rho_k\varphi(x,\tau)\,d\tau - \psi_k^\delta\Big).$$

since

$$\Big|\int_I p\rho_k(t)\Big(\int_0^S \rho_k\varphi(x,\tau)\,d\tau - \psi_k^\delta\Big)\Big| \le c'\Big(\Big\|\psi_k^\delta\Big\|_{\mathcal{L}^\infty(\chi)}\Big\|\rho_k\Big\|_{\mathcal{L}^\infty(0,S)} + \Big\|\rho_k\Big\|^2_{\mathcal{L}^\infty(0,S)}\Big\|\varphi\Big\|_{\mathcal{L}^\infty(\mathbf{I})}\Big)\Big\|p\Big\|_{\mathcal{L}^2(I)},$$

dividing by $\Big\|p\Big\|_{\mathcal{L}^2(I)}$, we find that

$$\Big\|p\Big\|_{\mathcal{L}^2(I)} \le c' \sum_{k=1}^{2} \Big\|\rho_k\Big\|_{\mathcal{L}^\infty(0,S)} \Big(\Big\|\psi_k^\delta\Big\|_{\mathcal{L}^\infty(\chi)} + \Big\|\rho_k\Big\|_{\mathcal{L}^\infty(0,S)} \Big\|\varphi\Big\|_{\mathcal{L}^\infty(\mathbf{I})}\Big).$$

this proves Lemma 3. □

Theorem 4. *The functional $\mathcal{M}[b, u_0]$ is Fréchet differentiable, and its gradients are given respectively by*

$$\nabla\mathcal{M}_b[b, u_0] = -\int_0^S \varphi(x,t)\,p(x,t)\,dt, \forall x \in \chi, \tag{37}$$

$$\nabla \mathcal{M}_{u_0}[b, u_0] = p(x, 0), \forall x \in \chi, \tag{38}$$

such that p is the solution to the adjoint problem (35).

Proof. Let δb be a small perturbation of b such that $b + \delta b \in \mathcal{E}$, denoted by $\delta u_b = \varphi(b + \delta b, u_0) - \varphi(b, u_0)$. Then, δb is the solution to the the following problem

$$\begin{cases} \partial_{tt}\delta\varphi_b - \nabla \cdot (a\,\nabla\delta\varphi_b) + b\,\delta b\delta\varphi_b + \delta b\varphi(b + \delta b, u_0) &= 0 \quad \text{in} \quad I, \\ \delta\varphi_b &= 0 \quad \text{in} \quad (\mathbb{R}^d \backslash \chi) \times (0, S], \\ \delta\varphi_b(\cdot, 0) &= 0 \quad \text{in} \quad \chi, \\ \partial_t\delta\varphi_b(\cdot, 0) &= 0 \quad \text{in} \quad \chi, \end{cases} \tag{39}$$

Then, we have

$$\begin{aligned} \mathcal{M}[b + \delta b, u_0) - \mathcal{M}[b, u_0) &= \int_I \delta u_b \left[\rho_1(t) \left(\int_0^S \rho_1 \varphi(x, \tau)\, d\tau - \psi_1^\delta \right) + \rho_2(t) \left(\int_0^S \rho_2 \varphi(x, \tau)\, d\tau - \psi_2^\delta \right) \right] \\ &\quad + \frac{1}{2} \sum_{k=1}^{2} \left\| \int_0^S \rho_k(t) \delta\varphi_b \right\|^2_{\mathcal{L}^2(\chi)} \\ &= -\partial_{tt} p - \nabla \cdot (a\,\nabla p) + bp + \frac{1}{2} \sum_{k=1}^{2} \left\| \int_0^S \rho_k(t) \delta\varphi_b(., \tau)\, d\tau \right\|^2_{\mathcal{L}^2(\chi)}. \end{aligned}$$

Using problems (35) and (39) and integrating over I, we obtain

$$\begin{aligned} \int_I \delta u_b \left(-\partial_{tt} p - \nabla \cdot (a\,\nabla p) + bp \right) &= \int_I p \left((\partial_{tt}\delta\varphi_b - \nabla \cdot (a\,\nabla\delta\varphi_b) + b\,\delta\varphi_b) \right) \\ &= -\int_I p\,\delta b\,\varphi(b + \delta b, u_0) \\ &= -\int_I p\,\delta b\,\delta\varphi_b - \int_I p\,\delta b\,\varphi(b, u_0). \end{aligned}$$

Hence,

$$\mathcal{M}[b + \delta b, u_0) - \mathcal{M}[b, u_0) = -\int_I p\,\delta b\,\delta\varphi_b - \int_I p\,\delta b\,\varphi(b, u_0) + \frac{1}{2} \sum_{k=1}^{2} \left\| \int_0^S \rho_k(t) \delta\varphi_b(., \tau)\, d\tau \right\|^2_{\mathcal{L}^2(\chi)}.$$

According to an estimate similar to that of (5) for $\delta\varphi_b$, we have

$$\left\| \int_0^S \rho_k(t) \delta\varphi_b(., \tau)\, d\tau \right\|^2_{\mathcal{L}^2(\chi)} \leq c \|\rho_k(t)\|_{\mathcal{L}^\infty(0,S)} \|\delta b\|_{\mathcal{L}^\infty(\chi)},$$

and

$$\left| \int_I p\,\delta b\,\delta\varphi_b \right| \leq c \|\delta b\|^2_{\mathcal{L}^\infty(\chi)} \|p\|_{\mathcal{L}^2(I)}.$$

Therefore,

$$\mathcal{M}[b + \delta b, u_0) - \mathcal{M}[b, u_0] = \int_\chi \left(\int_0^S -p\varphi\, dt \right) dx.$$

Hence,

$$\nabla \mathcal{M}_b[b, u_0] = -\int_0^S \varphi(x, t)\, p(x, t)\, dt, \forall x \in \chi.$$

Using the same approach used to calculate the gradient with respect to b, we calculate the gradient with respect to the initial condition u_0, such that the direct solution $\delta\varphi_{u_0} = \varphi(b, u_0 + \delta u_0 - \varphi(b, u_0)$ is the solution to the following problem

$$\begin{cases} \partial_{tt}\delta\varphi_{u_0} - \nabla\cdot(a\,\nabla\delta\varphi_{u_0}) + b\,\delta\varphi_{u_0} &= 0 & \text{in} & I, \\ \delta\varphi_{u_0} &= 0 & \text{in} & (\mathbb{R}^d\backslash\chi)\times(0,S], \\ \delta\varphi_{u_0}(\cdot,0) &= \delta u_0(x) & \text{in} & \chi, \\ \partial_t\delta\varphi_{u_0}(\cdot,0) &= 0 & \text{in} & \chi, \end{cases} \tag{40}$$

so we find (38). □

3. Conjugate Gradient Method

To reconstruct simultaneously the coefficient b and the initial condition u_0, we apply a process based on the conjugate gradient method (CGM), which consists of minimizing the functional in Equation (25). This process is given by:

$$b^{i+1} = b^i + \beta_b^i\gamma_b^i,\;\; u_0^{i+1} = u_0^i + \beta_{u_0}^i\gamma_{u_0}^i \;\; i = 0, 1, \cdots, \tag{41}$$

where $b^0(x), u_0^0(x)$ are the initial guesses for $b(x), u_0(x)$ where i is the number of iterations, and β^i denotes the step size. Moreover, we define the search directions γ_b^i and $\gamma_{u_0}^i$ by

$$\gamma_b^i = \begin{cases} -\nabla\mathcal{M}_b^0 & for \quad i = 0, \\ -\nabla\mathcal{M}_b^i + \rho_b^i\nabla\mathcal{M}_b^{i-1} & for \quad i \geq 1, \end{cases} \gamma_{u_0}^i = \begin{cases} -\nabla\mathcal{M}_{u_0}^0 & for \quad i = 0, \\ -\nabla\mathcal{M}_{u_0}^i + \rho_{u_0}^i\nabla\mathcal{M}_{u_0}^{i-1} & for \quad i \geq 1, \end{cases} \tag{42}$$

Additionally, we can use Fletcher–Reeves formula in [33] to obtain the step sizes $\beta_b^i, \beta_{u_0}^i$

$$\rho_b^i = \frac{\|\nabla\mathcal{M}_b^i\|_{\mathcal{L}^2(\chi)}}{\left\|\nabla\mathcal{M}_b^{i-1}\right\|_{\mathcal{L}^2(\chi)}}, \rho_{u_0}^i = \frac{\|\nabla\mathcal{M}_{u_0}^i\|_{\mathcal{L}^2(\chi)}}{\left\|\nabla\mathcal{M}_{u_0}^{i-1}\right\|_{\mathcal{L}^2(\chi)}}, \quad for \;\; i = 1, 2, \cdots. \tag{43}$$

In the same way, we can find β_b^i and $\beta_{u_0}^i$

$$\mathcal{M}(b^{i+1}, u_0^{i+1}) = \min_{\beta_b, \beta_{u_0}\geq 0}\mathcal{M}(b^i + \beta_b\gamma_b^i, u_0^i + \beta_{u_0}\gamma_{u_0}^i). \tag{44}$$

According to the arguments used in [34], the fact that $\nabla_b(b, u_0)$, $\nabla_{u_0}(b, u_0)$ is Frécher differentiable, and the fact that the functional $\mathcal{M}(b^{i+1}, u_0^{i+1})$ is a monotone decreasing convergent sequence, we obtain the following result:

Theorem 5. *The CGM (41)–(44) either terminates at a stationary point or converges in the following senses:*

$$\liminf_{i\to\infty}\|\nabla_b(b, u_0)\|_{L^2(\chi)} = \liminf_{i\to\infty}\|\nabla_{u_0}(b, u_0)\|_{L^2(\chi)}. \tag{45}$$

Since the errors can be noticed at the average weighted integral observations (3) and (4). The iteration process given by (42) cannot be preformed by the conjugate gradient method, and so the method is not well-posed because we do not have the regularization term. However, the method can become well-posed if we apply a divergence criterion so that the iteration procedure is stopped. This criterion is given by:

$$\mathcal{M}(b, u_0) \leq \frac{1}{2}\left\|\psi^\delta - \psi\right\|^2_{\mathcal{L}^2(\chi)} \leq \delta^2. \tag{46}$$

Thus, the iterations of this algorithm, based on CGM for the numerical reconstruction of the coefficient $b(x)$ and the initial condition $u_0(x)$, are as given by Algorithm 1.

Algorithm 1 CG algorithm for the minimizer of (25)

1. Set $i = 0$ and initiate b^0 and u_0^0 for the coefficient b and initial condition u_0.
2. Determine numerically, using the finite difference method, the solution to the direct problem (1) $\varphi(x, t, b^i, u_0^i)$ and the objective functional (25).
3. Determine numerically, using the finite difference method, the solution to the adjoint problem (35) $p(x, t, b^i, u_0^i)$ and the gradient of the objective functional (37) and (38). Calculate the coefficients $(\rho_b^i, \rho_{u_0}^i)$ and $(\gamma_b^i, \gamma_{u_0}^i)$ given in Equations (43) and (42), respectively.
4. Determine numerically, using the finite difference method, the solution to the sensitivity problems (39) and (39) $\delta\varphi_b(x, t, b^i, u_0^i)$ and $\delta\varphi_{u_0}(x, t, b^i, u_0^i)$ by using $\delta\varphi_b^i = \gamma_b^i$ and $\delta\varphi_{u_0}^i = \gamma_{u_0}^i$, where the step sizeS β_b^i and $\beta_{u_0}^i$ are given in (44)
5. Update b^i, u_0^i using (41).
6. If the condition (46) is satisfied, go to Step 7 . Else, set $i = i + 1$ and return to Step 2.
7. End.

4. Numerical Experiments

Here, we apply the CG method [35] in one and two dimensions in order to identify simultaneously the coefficient b and the initial condition u_0 in 1. We discretize this problem using the finite element method in space and the Crank–Nicholson scheme in time direction. For the two-dimensional problem, we apply the alternating direction implicit (ADI) method as described in [28]. We create the noisy data, and a random perturbation is added, i.e.,

$$\psi_1^\delta(x) = \psi_1 + \eta \times random(1), \quad \psi_2^\delta(x) = \psi_2 + \eta \times random(1),$$

where $\eta = p/100 \times \max_{x\in\chi}\{|\psi_1|, |\psi_2|\}$, and p represents the percentage of noise.

We calculate the approximate $\mathcal{L}^2$ error by the following formula to demonstrate the precision of the numerical solution

$$E_b^i = \left\| b^i - b^{\text{ex}} \right\|_{\mathcal{L}^2(\chi)}, \tag{47}$$

$$E_{u_0} = \left\| u_0^i - u_0^{\text{ex}} \right\|_{\mathcal{L}^2(\chi)}, \tag{48}$$

where (b^i, u_0^i) are the initial guesses reconstructed at the kth iteration, and $(b^{\text{ex}}, u_0^{\text{ex}})$ are the exact values. The residual R^i at the ith iteration is given by

$$R_1^i = \left\| u(b^i) - \psi_1^\delta \right\|_{\mathcal{L}^2(\chi)}, \quad R_2^i = \left\| u(u_0^i) - \psi_2^\delta \right\|_{\mathcal{L}^2(\chi)}.$$

4.1. One-Dimensional Problem

We fix $\chi = [0, 1]$ without a loss of generality. We also fix $\delta t = \frac{1}{100}$ and $\delta x = \frac{1}{100}$, respectively, and let $a(x) = (x - 0.5)^2$. We choose $\rho_1(t)$ and $\rho_2(t)$ in (3) and (4) as

$$\rho_i(t) = \frac{1}{q\sqrt{\pi}} \exp\left(-\frac{(t - t_i)^2}{10^{-6}}\right) \quad t \in [0, S], \quad i = 1, 2, \tag{49}$$

where q is a small positive constant, and $t_1 \neq t_2 \in [0, S]$. It is clear that $\rho_i(t) \approx \delta(t - t_i)$ for small values of q, where $\delta(.)$ is the Dirac delta function. Then, according to the properties of the Dirac delta function, Equations (3) and (4)would become

$$\psi_i = \int_0^S \rho_i(t)\varphi(x, t) \approx \int_0^S \delta(t - t_i)\varphi(x, t) = \varphi(x, t).$$

For all the three numerical examples presented later, we choose the weight functions as

$$\rho_1(t) = \frac{1000}{\sqrt{\pi}} \exp\left(-\frac{(t-0.3)^2}{10^{-6}}\right), \quad \rho_2(t) = \frac{1000}{\sqrt{\pi}} \exp\left(-\frac{(t-1)^2}{10^{-6}}\right).$$

Example 1. *To validate this choice, we apply our proposed algorithm for the reconstruction of the coefficient and the initial condition defined on* χ *by*

$$b^{\text{ex}}(x) = 1 + x^2, \;\; u_0^{\text{ex}}(x) = x(1-x). \tag{50}$$

We take the initial guesses $b^0(x) = 1$, $u_0^0(x) = 0$.

Figure 1 is devoted to showing the variation of the functional according to the number of iterations i for the simultaneous determination of the coefficient b and the initial condition u_0, in the cases of no noise $(p = 0)$ and with noise $(p = 1)$, $(p = 5)$. It can be observed that if $p = 0$, then the function $\mathcal{M}(b, u_0)$ quickly converges to a very small value because it is a decreasing function according to the values of i. We see that the number of iterations for the algorithm to stop is $i^* = 20$ in the case of no noise and $i^* = 3$ in the case of noise. These numbers of iterations are obtained via the discrepancy in (46). Errors (47) and (48) associated with $b(x)$ and $u_0(x)$ have been found for $E_b = 0.00008/0.0284/0.0274$ and $E_{u_0} = 0.000025/0.00322/0.00223$ with the noise levels $p = 0/1/5$, respectively. Therefore, we can conclude that our numerical process is reasonably accurate in determining the coefficient $b(x)$ and the initial condition $u_0(x)$. Similarly, the norms of the gradients of the functional are obtained for $\|\nabla \mathcal{M}_b\|_{\mathcal{L}^2(\chi)} = 2 \times 10^{-5}/0.0009/0.0014$ and $\left\|\nabla \mathcal{M}_{u_03}\right\|_{\mathcal{L}(2(\chi)} = 1.64 \times 10^{-5}/0.00018/0.00015$ with $p = 0/1/5$.

In Figure 2, we illustrate the comparison between the functions of the recovered coefficient b and the initial condition u_0 and their exact values with the noise levels $p = 0/1/5$.

Figure 2 illustrates the numerical reconstruction of the coefficient b and the initial condition u_0 with the number of final iterations i^* given in Figure 1 with different values for the noise levels, $p = 0/1/5$. From Figure 1, we can notice that the exact and the numerical solutions are almost equal; that is, the proposed algorithm to determine the two coefficients converges to the required solutions.

(a)

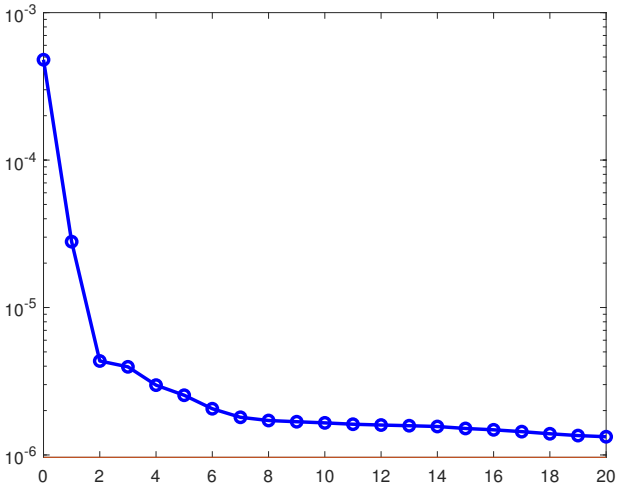

Figure 1. *Cont.*

(**b**)

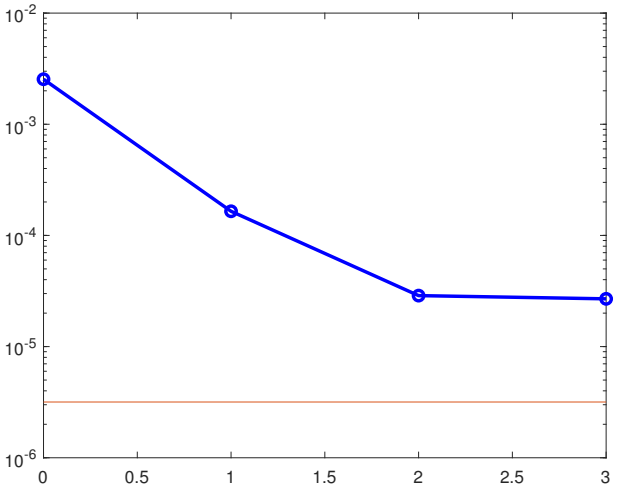

(**c**)

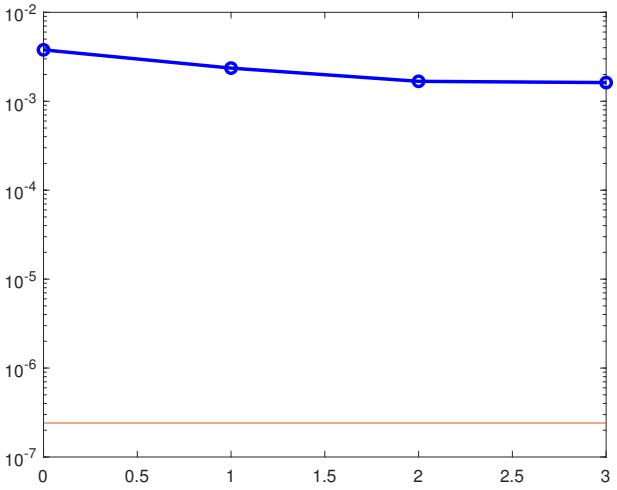

Figure 1. Graph of the functional $\mathcal{M}(b^i, u_0^i)$ to Example 1 with (**a**) $p = 0$; (**b**) $p = 1$; (**c**) $p = 5$.

In the following example, we will apply our method to reconstruct the coefficient b and the initial condition defined by

Example 2. *We consider*

$$b^{\text{ex}}(x) = x^3 + \sin(\pi x), \;\; u_0^{\text{ex}}(x) = \sin(\pi x). \tag{51}$$

Similarly, for Example 1, using the discrepancy in (46), the stopping iterations are, $i^* = 20/3/3$ for the noise levels $p = 0, 1$, and 5. The errors (47) and (48) associated with $b(x)$ and $u_0(x)$ have been found for $E_b = 0.000025/0.0081/0.0092$ and $E_{u_0} = 0.00018/0.00254/0.00353$ with noise level $p = 0, 1$ and 5, respectively, Under these stopping iterations, Figure 3 illustrates the exact and numerical solutions for Example 2 for different values of the noise levels ($p = 0, 1$, and 5).

(**a**)

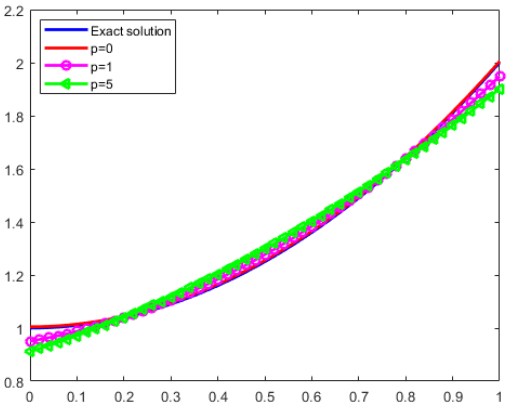

(**b**)

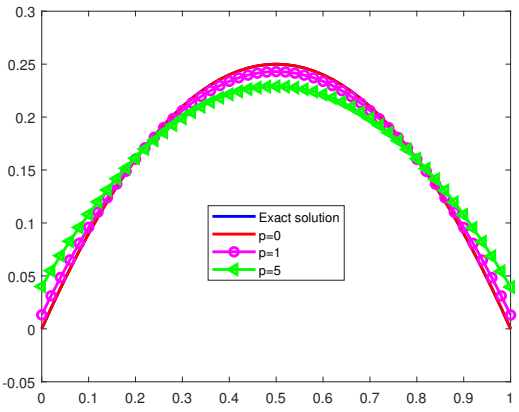

Figure 2. Reconstruction results for Example 1 with $p = 0, 1$, and 5. (**a**) coefficient b; (**b**) the initial condition u_0.

(**a**)

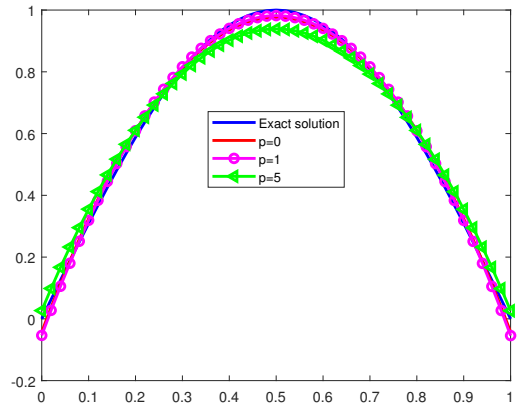

Figure 3. *Cont.*

(**b**)

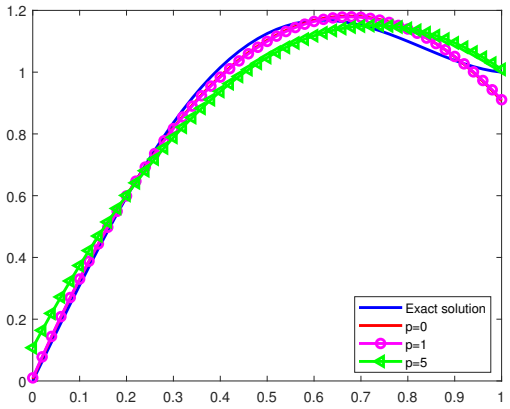

Figure 3. Reconstruction results for Example 2 with $p = 0, 1$, and 5. (**a**) coefficient b; (**b**) the initial condition u_0.

4.2. Two-Dimensional Problem

The space–time region $\chi \times [0, S] := [0, 1]^2 \times [0, 1]$ is partitioned into $40 \times 40 \times 80$ equidistant meshes. We testify the numerical performance of the Algorithm 1 for the reconstruction of the coefficient b and the initial condition b with the following degeneracy

$$a(\mathbf{x}) := a(x_1, x_2) = \sqrt{(x_1 - 0.3)^2 + (x_2 - 0.3)^2}. \tag{52}$$

We take the initial guesses $b^0(x_1, x_2) = 1$, $u_0^0(x_1, x_2) = 0$.

Example 3. *Suppose that the exact coefficient and initial condition for the degenerate wave problem (1) are given by:*

$$b^{\text{ex}}(x_1, x_2) = \cos(2\pi x_1)\cos(3x_2), \;\; u_0^{\text{ex}}(x_1, x_2) = (1 - x_2)\sin(\pi x_1). \tag{53}$$

For this example, the number of the final iterations of CGM is $i^* = 60/3/3$, for the noise levels $p = 0, 1$, and 5 (Figure 4). Errors (47) and (48), associated with $b(x)$ and $u_0(x)$, have been found for $E_b = 0.01, 0.05$, and 0.21. Additionally, $E_{u_0} = 0.051, 0.154$, and 0.254.

(**a**)

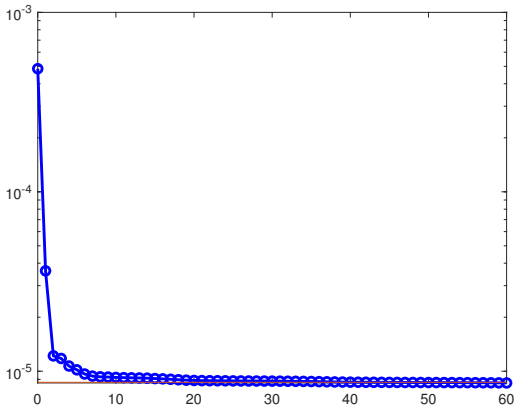

Figure 4. *Cont.*

(**b**)

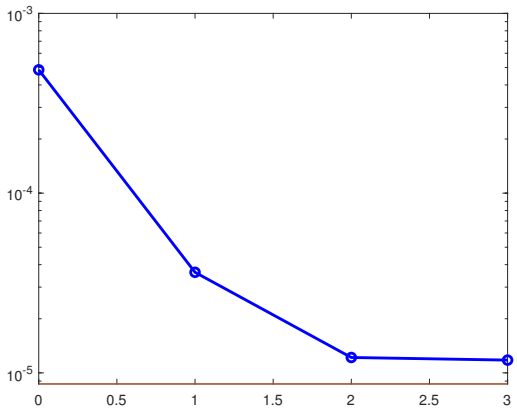

(**c**)

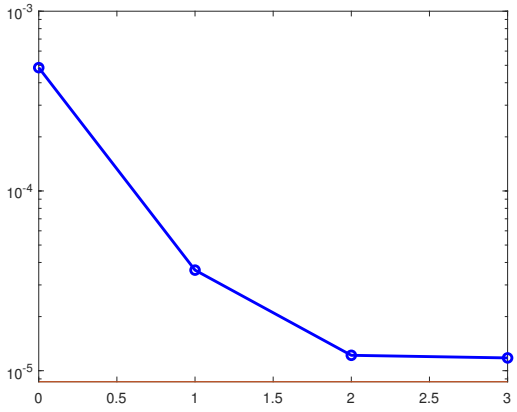

Figure 4. Graph of the functional $\mathcal{M}(b^i, u_0^i)$ for Example 3 with (**a**) $p = 0$; (**b**) $p = 1$; (**c**) $p = 5$.

The exact coefficient, initial condition functions, and recovered solution are shown in Figures 5 and 6.The absolute errors between the exact coefficient and initial condition functions and their numerical reconstruction are shown in Figures 7 and 8.We can notice that the recovered terms are very close to the exact solutions; this shows the effectiveness of our proposed method.

The following Tables 1 and 2 are devoted to the different values of E_b^i and $E_{u_0}^i$ for $p = 0$, $p = 1$, and $p = 5$.

Table 1. Numerical results (accuracy error E_b^i).

	$p = 0$	$p = 1$	$p = 5$
Example 1	0.00008	0.0284	0.0377
Example 3	0.000025	0.003020	005040
Example 3	0.01	0.05	0.21

Table 2. Numerical results (accuracy error $E_{u_0}^i$).

	$p = 0$	$p = 1$	$p = 5$
Example 1	0.00025	0.00322	0.00524
Example 3	0.00221	0.00102	0.00417
Example 3	0.051	0.0254	0.0354

Here, we summarize the results of the numerical experiments. For one-dimensional problems, as considered in Example 1, the resulting figures can be described as follows. Figure 1a represents the graph of the functional $\mathcal{M}$ without a noise level (0 percent) and with the iteration number $i^* = 20$, while Figure 1b represents the graph of the functional $\mathcal{M}$ with a noise level (1 percent) with the number of iterations $i^* = 3$, Figure 1c represents the graph of the functional $\mathcal{M}$ with a noise level (5 percent) with the number of iterations $i^* = 3$. Figure 2a represents the graph of the reaction coefficient b without a noise level (0 percent) and with a noise level (1 and 5 percent). Additionally, Figure 2b represents the graph of the initial condition u_0 without a noise level (0 percent) and with a noise level (1 and 5 percent). For Example 2, Figure 3a represents the graph of the reaction coefficient b without a noise level (0 percent) and with a noise level (1 and 5 percent). Moreover, Figure 3b represents the graph of the initial condition u_0 without a noise level (0 percent) and with a noise level (1 and 5 percent).

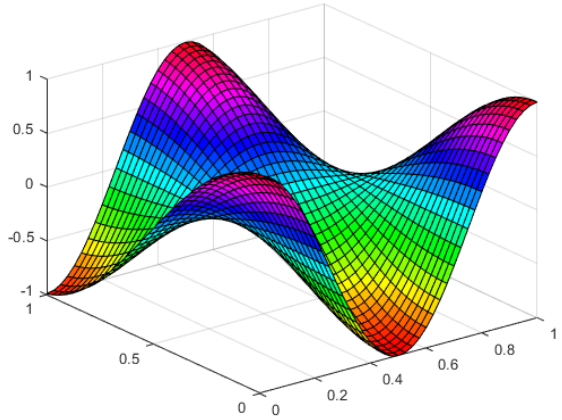

Figure 5. True coefficient function (53) for Example 3.

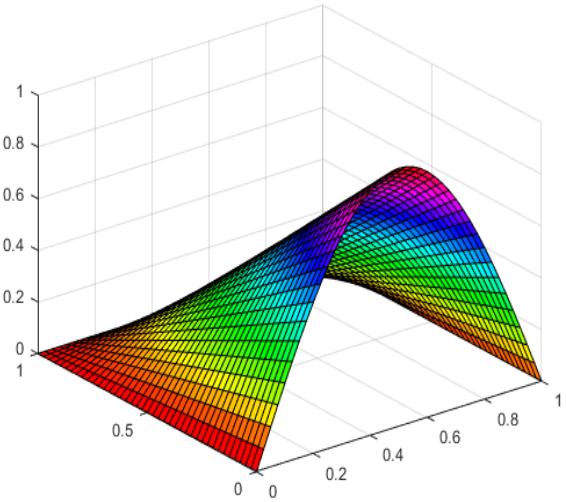

Figure 6. True initial condition function (53) for Example 3.

(**a**)

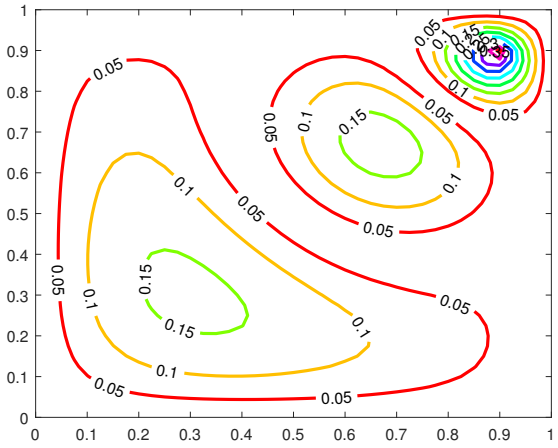

(**b**)

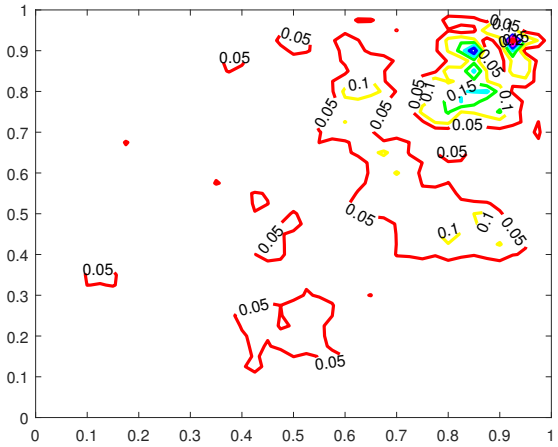

(**c**)

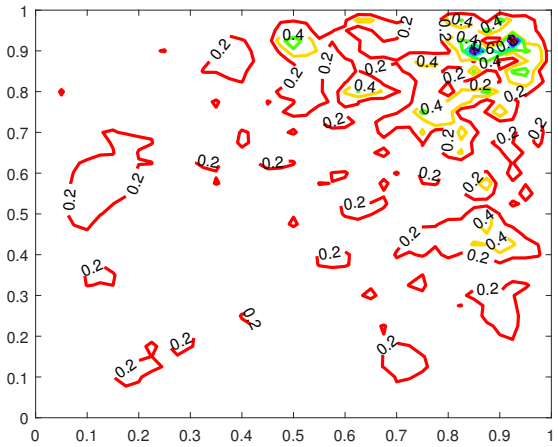

Figure 7. Absolute error between exact and numerical coefficient b with different noise levels (**a**) $p = 0$; (**b**) $p = 1$; (**c**) $p = 5$ for Example 3.

(**a**)

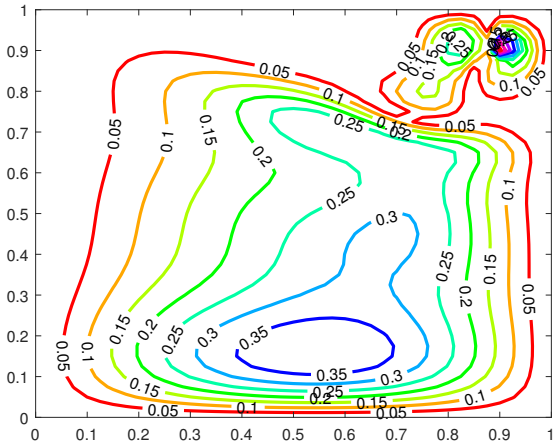

(**b**)

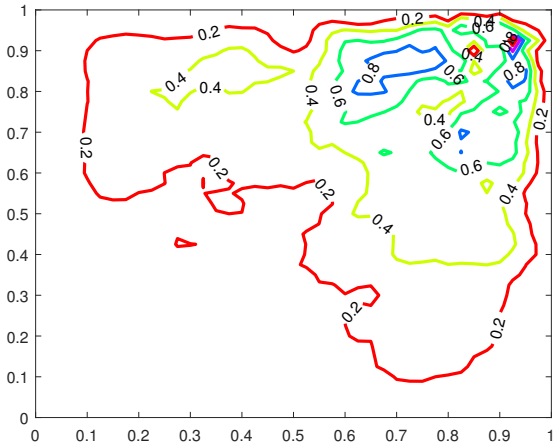

(**c**)

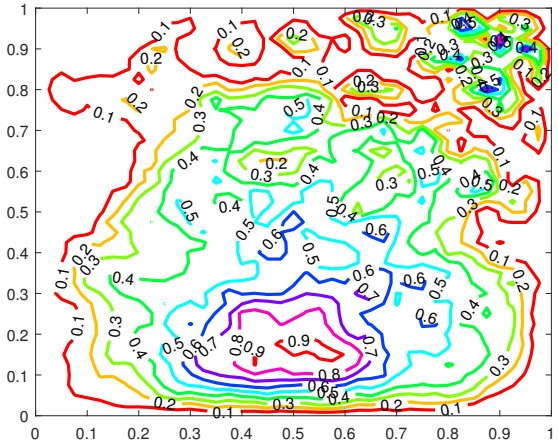

Figure 8. Absolute error between exact and numerical initial condition u_0 with different noise levels (**a**) $p = 0$; (**b**) $p = 1$; and (**c**) $p = 5$ for Example 3.

For two-dimensional problems, as given in Example 3, Figure 4a represents the graph of the functional $\mathcal{M}$ without a noise level (0 percent) and with the iteration number $i^* = 60$. Figure 4b represents the graph of the functional J with a noise level (1 percent) and with the number of iterations $i^* = 3$. Figure 4c represents the graph of the functional J with a noise level (5 percent) and with the number of iterations $i^* = 3$. Figure 5 represents the exact solution to the recovered reaction coefficient. Figure 9a, Figure 9b, and Figure 9c represent the graphs of the reaction coefficient b without a noise level (0 percent) and with noise levels (1 and 5 percent), respectively. Figure 7a, Figure 7b, and Figure 7c represent the graphs of the absolute error between the exact and numerical reaction coefficient b without a noise level (0 percent) and with noise levels (1 and 5 percent), respectively . Figure 6 gives the exact solution to the initial condition. Figure 10a, Figure 10b, and Figure 10c represent the graph of the reaction coefficient b without a noise level (0 percent) and with noise levels (1 and 5 percent), respectively. Figure 8a, Figure 8b, and Figure 8c represent the graphs of the absolute error between the exact and numerical reaction coefficient b without a noise level (0 percent) and with noise levels (1 and 5 percent), respectively.

(**a**)

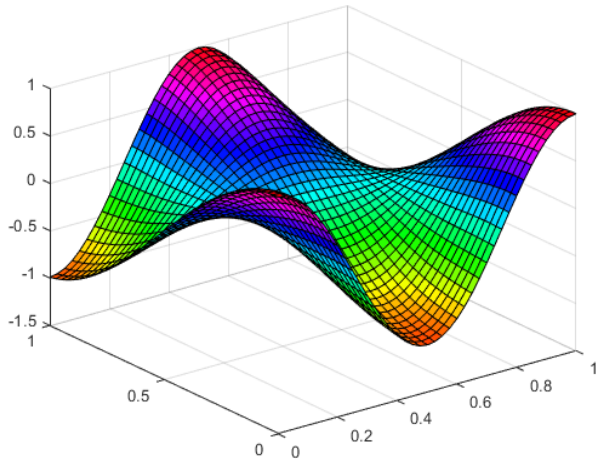

(**b**)

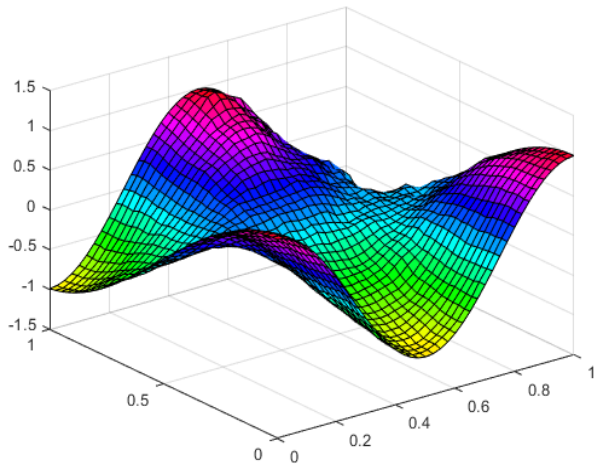

Figure 9. *Cont*.

(**c**)

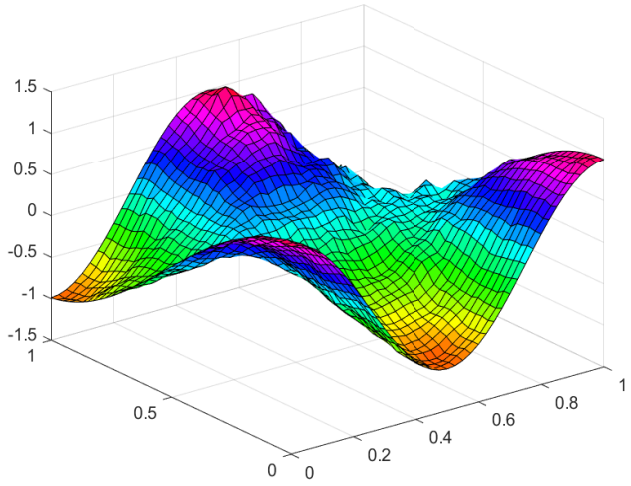

Figure 9. Numerical coefficient function reconstruction results for Example 3 with different noise levels (**a**) $p = 0$; (**b**) $p = 1$; (**c**) $p = 5$.

(**a**)

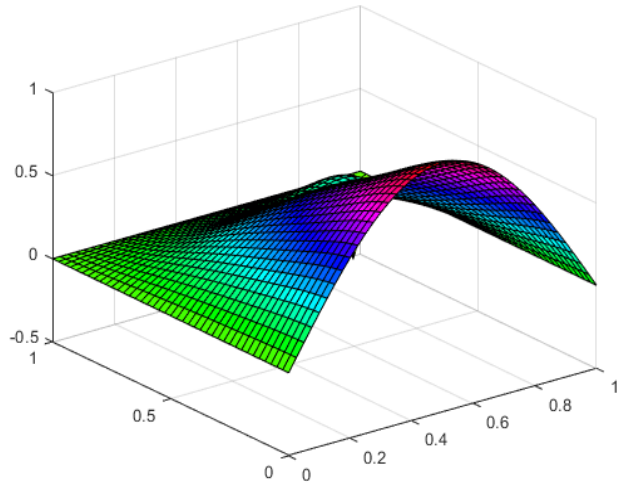

(**b**)

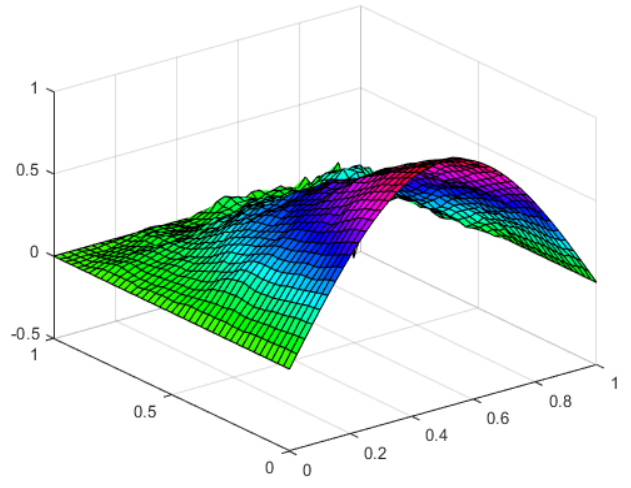

Figure 10. *Cont.*

(**c**)

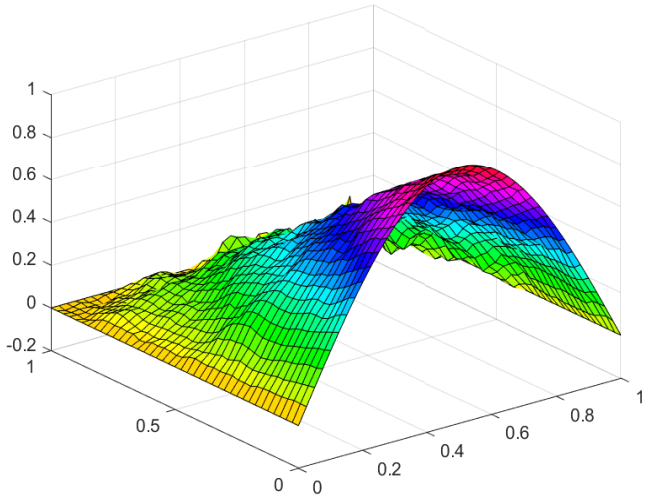

Figure 10. Numerical initial condition function reconstruction results for Example 3 with different noise levels (**a**) $p = 0$; (**b**) $p = 1$; (**c**) $p = 5$.

5. Conclusions

In this article, we were concerned with the simultaneous determination of the reaction coefficient, which depends on space, and the initial condition of a hyperbolic problem with degeneracy within the spatial domain from temporal integral observations. The existence, uniqueness, and stability of the inverse problem are examined. The CG conjugate gradient method has been proposed with adjoint and sensitivity problems for simultaneously reconstruction of the two unknown functions by minimizing the objective least squares functional. In the simulation part, we consider some numerical experiments in which we reconstruct numerically the initial condition and potential for wave problems in one and two dimensions.

Author Contributions: Conceptualization, H.O.S., M.A.Z., R.H.d.S. and A.S.H.; Formal analysis, H.O.S., M.A.Z., R.H.d.S. and A.S.H.; Funding acquisition, R.H.d.S. and A.S.H.; Methodology, H.O.S., M.A.Z., R.H.d.S. and A.S.H.; Supervision, R.H.d.S. and A.S.H.; Visualization, H.O.S. and M.A.Z.; Writing—original draft, H.O.S., M.A.Z. and A.S.H.; Writing—review and editing, R.H.d.S. All authors have read and agreed to the published version of the manuscript.

Funding: Ahmed Hendy wishes to acknowledge the RSF, Russia grant, project 22-21-00075.

Data Availability Statement: Not applicable.

Acknowledgments: We thank the respected reviewers for their valuable comments which significantly improved the paper.

Conflicts of Interest: The authors declare no conflict of interest. The funders had no role in the design of the study; in the collection, analyses, or interpretation of data; in the writing of the manuscript; or in the decision to publish the results.

References

1. Frisch, U.; Matarrese, S.; Mohayaee, R.; Sobolevski, A. A reconstruction of the initial conditions of the universe by optimal mass transportation. *Nature* **2002**, *417*, 260–262. [CrossRef] [PubMed]
2. Kalnay, E. *Atmospheric Modeling, Data Assimilation and Predictability*; Cambridge University Press: Cambridge, UK, 2003.
3. Rodgers, C.D. *Inverse Methods for Atmospheric Sounding: Theory and Practice*; World Scientific: Singapore, 2000; Volume 2.
4. Kuchment, P.; Kunyansky, L. Mathematics of thermoacoustic tomography. *Eur. J. Appl. Math.* **2008**, *19*, 191–224. [CrossRef]
5. Gouveia, W.P.; Scales, J.A. Bayesian seismic waveform inversion: Parameter estimation and uncertainty analysis. *J. Geophys. Res. Solid Earth* **1998**, *103*, 2759–2779. [CrossRef]
6. Beauchard, K.; Zuazua, E. Some controllability results for the 2D Kolmogorov equation. In *Annales de l'IHP Analyse Non Linéaire*; Elsevier: Paris, France, 2009; Volume 26, pp. 1793–1815.

7. Buchot, J.M.; Raymond, J.P. A linearized model for boundary layer equations. In Proceedings of the Optimal Control of Complex Structures: International Conference in Oberwolfach, 4–10 June 2000; Springer: Berlin/Heidelberg, Germany, 2002; pp. 31–42.
8. Shimakura, N. *Partial Differential Operators of Elliptic Type*; Translated from Japanese by N. Shimakura; American Mathematical Society: Providence, RI, USA, 1992.
9. Zaky, M.A.; and Taha, T.R.; and Suragan, D.; Hendy, A.S. An L1 type difference/Galerkin spectral scheme for variable-order time-fractional nonlinear diffusion–reaction equations with fixed delay. *J. Comput. Appl. Math.* **2023**, *420*, 114832. [CrossRef]
10. Hendy, A.S.; De Staelen, R.H.; Aldraiweesh, A.A.; Zaky, M.A. High order approximation scheme for a fractional order coupled system describing the dynamics of rotating two-component Bose-Einstein condensates. *AIMS Math.* **2023**, *8*, 22766–22788. [CrossRef]
11. Ameen, I.G.; Zaky, M.A.; Doha, E.H. Singularity preserving spectral collocation method for nonlinear systems of fractional differential equations with the right-sided Caputo fractional derivative. *J. Comput. Appl. Math.* **2021**, *392*, 113468. [CrossRef]
12. Hendy, A.S.; Van Bockstal, K. On a reconstruction of a solely time-dependent source in a time-fractional diffusion equation with non-smooth solutions. *J. Sci. Comput.* **2022**, *90*, 41. [CrossRef]
13. Hendy, A.S.; Van Bockstal, K. A solely time-dependent source reconstruction in a multiterm time-fractional order diffusion equation with non-smooth solutions. *Numer. Algorithms* **2022**, *90*, 809–832. [CrossRef]
14. Sidi, H.O.; Zaky, M.A.; Qiu, W.; Hendy, A.S. Identification of an unknown spatial source function in a multidimensional hyperbolic partial differential equation with interior degeneracy. *Appl. Numer. Math.* **2023**, *192*, 1–18. [CrossRef]
15. Petersson, N.A.; Sjögreen, B. Super-grid modeling of the elastic wave equation in semi-bounded domains. *Commun. Comput. Phys.* **2014**, *16*, 913–955. [CrossRef]
16. Tarantola, A. Inversion of seismic reflection data in the acoustic approximation. *Geophysics* **1984**, *49*, 1259–1266. [CrossRef]
17. Isakov, V. Inverse parabolic problems with the final overdetermination. *Commun. Pure Appl. Math.* **1991**, *44*, 185–209. [CrossRef]
18. Prilepko, A.I.; Kostin, A.B. On certain inverse problems for parabolic equations with final and integral observation. *Matematicheskii Sbornik* **1992**, *183*, 49–68. [CrossRef]
19. Kozhanov, A.I. A Nonlinear Loaded Parabolic Equation and a Related Inverse Problem. *Math. Notes* **2004**, *76*, 784–795 . [CrossRef]
20. Kamynin, V.; Kostin, A. Two inverse problems of finding a coefficient in a parabolic equation. *Differ. Equ.* **2010**, *46*, 375–386. [CrossRef]
21. Deng, Z.C.; Yang, L.; Yu, J.N. Identifying the radiative coefficient of heat conduction equations from discrete measurement data. *Appl. Math. Lett.* **2009**, *22*, 495–500. [CrossRef]
22. Chen, Q.; Liu, J. Solving an inverse parabolic problem by optimization from final measurement data. *J. Comput. Appl. Math.* **2006**, *193*, 183–203. [CrossRef]
23. Trucu, D.; Ingham, D.B.; Lesnic, D. Space-dependent perfusion coefficient identification in the transient bio-heat equation. *J. Eng. Math.* **2010**, *67*, 307–315. [CrossRef]
24. Cao, K.; Lesnic, D. Reconstruction of the space-dependent perfusion coefficient from final time or time-average temperature measurements. *J. Comput. Appl. Math.* **2018**, *337*, 150–165. [CrossRef]
25. Erdem, A.; Lesnic, D.; Hasanov, A. Identification of a spacewise dependent heat source. *Appl. Math. Model.* **2013**, *37*, 10231–10244. [CrossRef]
26. Johansson, B.T.; Lesnic, D. A procedure for determining a spacewise dependent heat source and the initial temperature. *Appl. Anal.* **2008**, *87*, 265–276. [CrossRef]
27. Yamamoto, M.; Zou, J. Simultaneous reconstruction of the initial temperature and heat radiative coefficient. *Inverse Probl.* **2001**, *17*, 1181. [CrossRef]
28. Cao, K.; Lesnic, D.; Liu, J. Simultaneous reconstruction of space-dependent heat transfer coefficients and initial temperature. *J. Comput. Appl. Math.* **2020**, *375*, 112800. [CrossRef]
29. Cao, K.; Lesnic, D. Simultaneous identification and reconstruction of the space-dependent reaction coefficient and source term. *J. Inverse Ill-Posed Probl.* **2021**, *29*, 867–894. [CrossRef]
30. Alifanov, O.M. *Inverse Heat Transfer Problems*; Springer Science & Business Media: Berlin/Heidelberg, Germany, 2012.
31. Atifi, K.; Essoufi, E.H.; Khouiti, B. New approach to identify the initial condition in degenerate hyperbolic equation. *Inverse Probl. Sci. Eng.* **2019**, *27*, 484–512. [CrossRef]
32. Engl, H.W.; Groetsch, C.W. Projection-regularization methods for linear operator equations of the first kind. In *Special Program on Inverse Problems*; Australian National University, Mathematical Sciences Institute: Canberra, Australia, 1988; Volume 17, pp. 17–32.
33. Fletcher, R.; Reeves, C.M. Function minimization by conjugate gradients. *Comput. J.* **1964**, *7*, 149–154. [CrossRef]
34. Dai, Y.H.; Yuan, Y.X. Convergence properties of the Fletcher-Reeves method. *Ima J. Numer. Anal.* **1996**, *16*, 155–164. [CrossRef]
35. Nazareth, J.L. Conjugate gradient method. *Wiley Interdiscip. Rev. Comput. Stat.* **2009**, *1*, 348–353. [CrossRef]